Residual Loading Capacity of Ultra-High Performance Concrete Columns After Blast Loads

Jun Li[1, *], Chengqing Wu[1] and Hong Hao[2]
[1]School of Civil, Environmental and Mining Engineering, the University of Adelaide, SA 5005, Australia
[2]Department of Civil Engineering, Curtin University, WA 6845, Australia

Received on 23 June 2015; Accepted 5 October 2015

ABSTRACT
Columns are essential load carrying structural components and may experience accidental loads such as terrorist bombing attacks during their service life. Damages to columns may trigger structural collapse and it is therefore very important to protect critical load-carrying columns. In recent studies, a novel ultra-high performance concrete (UHPC) material was developed and static loading test results revealed its outstanding mechanical strengths and ductility. The present study investigates the blast load-carrying capacities of columns made of UHPC. Concrete columns built with UHPC were blast tested in the field first; then brought back to laboratory and subjected to static load tests to determine their residual load-carrying capacities after experiencing varying levels of blast damage. The results from the field blast tests and laboratory static load tests for residual load-carrying capacities are presented and discussed in this paper. Numerical models for simulating responses and residual strengths of the UHPC columns after blast loadings are also developed in commercial hydro-code LS-DYNA and presented in the paper. Comparisons between the test data and numerical results are made and the accuracy of the numerical model is validated.

Key words: UHPC, column, blast test, residual strength, numerical simulation

1. INTRODUCTION

In contemporary society, concrete is the most widely used building material. Working together with steel reinforcement, concrete can provide a high level of loading capacity which allows construction of high-rise buildings. During their service life, other than the design loads, reinforced concrete structures may experience extreme loads from impacts or explosions. Under these extreme loading conditions, instant response including flexural damage, shear damage and concrete spall may occur. Subsequent damage to the entire

*Corresponding author. E-mail address: J.li@adelaide.edu.au

Figure 1. Structural progressive collapse induced by blast loads Left: 1995 Alfred P. Murrah Federal Building (http://en.wikipedia.org/wiki/Alfred_P._Murrah_Federal_Building) Right: 1968 Ronan Point Building (http://en.wikipedia.org/wiki/Ronan_Point)

building, which is known as progressive collapse (as shown in Figure 1), can then be triggered after damage to one or several key load carrying members occurs and there is insufficient redundant load paths. In recent years, the increase in terrorism activities highlights the importance of structural protection against blast loadings. Understanding the performance and remaining load-carrying capacities of structural columns after blast loadings is essential for structural protection.

Blast performance of structural members like concrete beams, columns and slabs has been extensive investigation [1–4] in recent years. Under blast loading conditions, structural components may fail in multiple modes. At large scaled distances, flexural failure with ductile structural behaviour and the maximum energy absorption may occur. With a decrease of scaled distance of blast scenarios, brittle damage modes like shear failure or combined shear and flexural failure may occur. When a blast occurs in close proximity to, or in contact with, concrete components, localized damage like concrete spall and cratering may happen. Under this condition, assessing damage is of importance and significance for structural protective design. Pressure-impulse diagrams are widely adopted for evaluating blast induced damage. A pressure-impulse diagram (P-I diagram) contains a series of iso-damage curves in which each iso-damage curve represents a structural damage level. Damage criterion for P-I diagrams should be carefully chosen depending on the blast loading conditions and corresponding damage types. For structures which experience global deformations under blast loading conditions, the structural central deflections have been adopted as the damage criterion. According to this criterion, Fallah and Louca [5] derived pressure–impulse diagrams for elastic–plastic hardening and elastic–plastic softening SDOF systems under blast loads. Li and Meng [6] studied the pulse loading shape effects on the pressure–impulse diagram based on the maximum deflection damage criterion and the elastic SDOF model. When considering brittle shear damage, Li and Hao [2, 7] used the shear slip close to the boundary to define the brittle shear damage level and generated P-I diagrams. Although these parameters provide good quantifications of column damages subjected to blast loadings, they are indirect assessment of column conditions in relation to the functionality of structural columns. Since the primary function of a structural column is to carry vertical load, a damage criterion based on remaining load-carrying capacity of RC

columns after blast loading was proposed by Shi et al. [8]. In the latter work, parametric studies were conducted to investigate the effects of column geometry, concrete strength, longitudinal and transverse reinforcement ratio on RC column capacity to resist blast loads. P-I diagrams were developed according to damage criteria defined with respect to the remaining load-carrying capacities. Based on the numerical results, analytical formulae to predict the P-I diagrams for RC columns were derived. These P-I diagrams give more direct and quantitative assessments of column functionality after blast loadings.

As discussed above, residual load-carrying capacity of columns plays a key role in the structural post blast performance. If residual load-carrying capacity is sufficient, the threat of progressive collapse can then be minimized. Bao and Li [9] utilized a verified Finite Element (FE) model to study the residual load-carrying capacity of a column after a blast. An extensive parametric study was carried out on a series of 12 columns to investigate the effects of transverse reinforcement ratio, axial load ratio, longitudinal reinforcement ratio, and column aspect ratio on the residual load-carrying capacity. Roller et al. [10] observed that there is little research regarding the behaviour of elements with one-dimensional load capacity like columns and their capacity under blast loading conditions. To provide more in-depth knowledge, they started a test program involving both standard reinforced concrete columns and retrofitted concrete columns under blast loads first and then static loads. Remaining load-carrying capacities of blast-damaged columns were obtained through uniaxial compressive tests.

Generally speaking, there are two ways to enhance the blast resistance capacity of concrete columns. The first one is to retrofit concrete columns with fibre reinforced polymer (FRP) composite laminates [11]. Hao et al. [12] carried out reliability analysis of RC columns with FRP strengthening under explosive loading conditions, and demonstrated the effectiveness of FRP strengthening on structural protection. Through extensive numerical simulations, Mutalib and Hao [13] developed P-I curves for assessing the damage of FRP retrofitted concrete columns after blast loads. Wu et al. [14] conducted blast tests on two reinforced concrete specimens: a plain reinforced concrete (RC) specimen; and an identical RC specimen retrofitted with near surface mounted (NSM) carbon fibre reinforced polymer (CFRP) plates. A number of unique behaviours of both specimens were observed, investigated and analysed.

Another effective method to enhance the blast resistance of columns is to use high performance concrete material such as ultra-high performance concrete (UHPC). Compared with normal strength concrete, UHPC is known for its high strength, high ductility and high durability. It allows construction of sustainable and economic buildings with extraordinarily slim designs. Its ultra-high strength and ductility makes it an ideal construction material for bridge decks, storage halls, thin-wall shell structures, and highly loaded columns. As a relatively new concrete material, optimization of the material composition of UHPC is still widely studied in order to cater for the need of even better performance such as early age workability, impact and explosive resistance, fire and corrosion resistance and aggressive chemical resistance. With the development of nano technology, researchers noticed that several phenomena including statistical mechanical effects and quantum mechanical effects become pronounced as the size of the system decreases. Addition of nanoscale size particles results in significantly improved material properties without much change of the material composition. Studies concerning properties of cement mortars with nano-SiO_2 addition was carried out [15]. The experimental results showed that the compressive strengths of mortars with nano-SiO_2 particles were all higher than those of mortars containing silica fume at 7 and 28 days. It was concluded that it was plausible to add nano-SiO_2 particles in order to make

high-performance concrete. Similar observations [16] were obtained and it was also noticed that comparing with cement paste with silica fume addition, the cement paste mixed with nano-SiO_2 particles had obviously higher compressive strength, especially at early age. Nano-SiO_2 was believed to accelerate the cement hydration process. These findings proved that addition of nano materials can increase the hydration process and thus enables an early age workability of UHPC. Liu et al. [17] added nano-$CaCO_3$ (NC) into the cement paste and they observed a decreased flowability and shortened setting time of fresh cement paste, and they also noticed that compressive strength of UHPC increased with the addition of NC at ages of 7 days and 28 days. Similar observations were also made through experimental studies in [18]. These findings indicate that the addition of small amount of nano materials can increase the mechanical performance of the UHPC material.

The development of UHPC is based on advancements in the materials science. Considerable effort is required to transfer and implement the knowledge gained at the material level to structural engineering and design. In previous studies, blast testing was conducted on UHPC slabs [19] and compared with control samples made with normal strength concrete. It was concluded that a combination of high strength concrete with steel fibre can significantly increase the explosive resistance of structural components. Impact response of UHPC material through drop weight tests was observed [20], and direct comparisons were made with conventional normal strength fibre reinforced concrete. Results indicated that UHPC was approximately two times stronger than normal strength fibre reinforced concrete.

In a recent study, a novel UHPC material with nano particle addition was developed, and static tests in the laboratory confirmed its outstanding mechanical performance compared to normal strength concrete [21]. To get in-depth knowledge of the blast resistance performance of this novel UHPC material, field blast tests were carried out on reinforced concrete columns made with this material [22]. The blast-damaged columns were then taken back to the laboratory and subjected to static tests to determine their residual load-carrying capacities. In this paper, field blast tests and laboratory residual load-carrying capacity tests are presented and discussed. Numerical model based on these test results is developed in commercial hydro-code LS-DYNA. Comparison of the numerical results with the test data is also presented.

2. BLAST TEST PROGRAM

The test specimens include two UHPC columns with 2.5 m span length, and rectangular cross section of 0.2 m × 0.2 m. The geometry of the UHPC columns, layout of the longitudinal reinforcements and spacing of the transverse reinforcement are shown in Figure 2. The threaded longitudinal reinforcement bar has a diameter of 16 mm and a yielding strength of 1450 MPa. The stirrup reinforcement is roller plain steel bar with a diameter of 8 mm and yielding strength of 300 MPa.

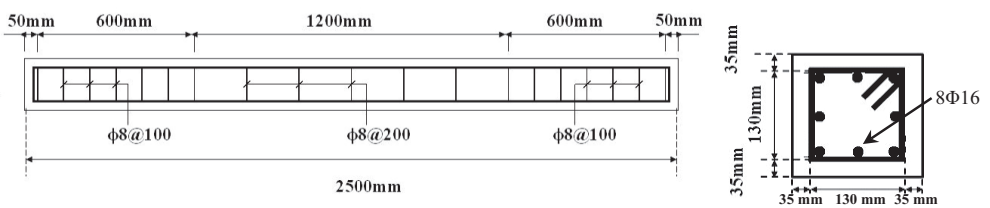

Figure 2. Configuration of UHPC columns

For UHPC material under investigation, micro steel fibre with 2.5% volume dosage and nano-$CaCO_3$ particles with 3% weight dosage are mixed in the concrete matrix to enhance its performance. Micro steel fibre has a length of 15 mm and diameter of 0.12 mm. The tensile strength for micro steel fibre is 4295 MPa. Stress strain relationship for this UHPC material under uniaxial compression test is shown in Figure 3. It is noted that adding micro fibre reinforcement and nano particle has greatly improved the UHPC compressive strength (around 148 MPa) and material ductility as compared with normal strength concrete.

The field blast testing arrangement is shown in Figure 4. The column specimen was placed on a steel supporting rig and then lowered to the ground level. Both ends of the column were fixed using steel bolts, and two strips of rubber sheet were used to cover the gaps between the column and ground support. This arrangement was proved effective in preventing the blast wave passing through the gaps, which might not only destroy the testing instruments beneath the column, but also result in shock waves engulfing the column specimen. Emulsion explosive, with an effectiveness factor 1.4, i.e. 1.4 kg Emulsion explosive equals 1 kg TNT, was used in the test. Explosive was hung over the column with a height of 1.5 m by a bamboo tripod.

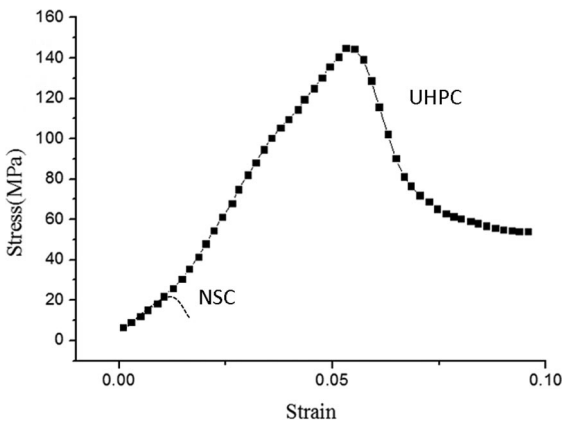

Figure 3. Stress-strain relationship of UHPC and NSC from uniaxial compressive test

Figure 4. Field blast testing system

Three LVDTs with a stroke of up to 300 mm were placed beneath the column on the distal surface to record the column deflections. All the LVDTs were attached to the column using a Dynabolt. The sample rate for the LVDTs was 0.2 MHz. For measuring the reflected pressure, the pressure transducers were installed at 0 mm, 380 mm and 760 mm away from the centre of the column specimen, respectively, as shown in Figure 4. The measuring range of the transducer was 0–70 MPa.

Two UHPC columns, i.e. U1B and U2B were tested in the program. For U1B column, two blast scenarios were considered, i.e., 1 kg TNT equivalent explosive was firstly detonated to record the response in the data acquisition sensors and check if all the sensors were working properly. After that a 17.5 kg TNT explosive was detonated. Axial load was not applied in these two blast scenarios. For U2B column, the same blast loading scenarios were applied. However, being different from U1B column, U2B column was loaded with a constant axial load of 1000 kN at column ends. The axial load was applied through the air jack located at column end as shown in Figure 4.

3. FIELD TEST RESULTS

The typical blast pressure curves obtained from field tests are shown in Figure 5. As expected, for pressure sensors located at different locations, the blast pressure and duration varies. Test results are summarised in Table 1. In this table the reflected pressure and impulse are obtained from the central pressure gauge P1 at column mid-span as indicated in Figure 4. For U1B column without axial load, the column under 17.5 kg TNT equivalent explosion at 1.5 m standoff distance had a maximum mid-span deflection of 63.74 mm and a residual

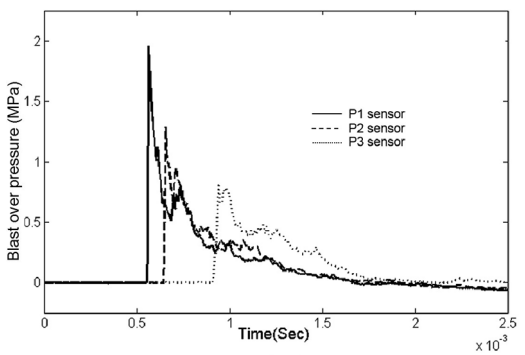

Figure 5. Typical recorded blast overpressure on UHPC column U1B corresponding to 1 kg TNT equivalent explosion

Table 1. Test results

Specimen	TNT equivalent (kg)	Axial load (kN)	Scaled distance ($m/kg^{1/3}$)	Maximum Reflected Pressure (MPa)	Maximum deflection (mm)	Residual deflection (mm)
U1B	1	0	1.5	1.9	1.96	0
U1B	17.5	0	0.58	29.01	63.74	18
U2B	1	1000	1.5	1.861	1.24	0
U2B	17.5	1000	0.58	–	29.27	4

Note: – indicates a faulty value.

deflection of 18 mm, and the ratio of maximum deflection to span length was 2.5%. With inclusion of 1000 kN axial load, under the same blast, the U2B column maximum central deflection was 29.27 mm, and the residual central deflection was merely 4 mm. The ratio of maximum deflection to span length was 1.2%. U2B had better performance than U1B in terms of the maximum central deflection and residual deflection. Both columns experienced ductile structural deformation.

The recorded deflection time histories of these two columns will be presented later together with the numerical simulation results.

Figure 6 shows U1B and U2B columns after blast tests. For U1B column, it is easily noted that minor flexural damage happened at mid span, and noticeable hairline cracks are seen on the bottom side of the column. The residual deflection for U1B column is around 18 mm. For U2B column, visible but not significant mid span cracks are noted as shown in the figure, and its residual deflection is small and around 4 mm.

It is worth noting that, column damage observed in the present study is different from previous full-scale structural tests [23, 24], and such deviation can be attributed to the column boundary setup. In real structures, longitudinal reinforcements in columns are extended into the foundation and beam or slab providing lateral and tensile resistance through shear and membrane effects (both compressive membrane and tensile membrane) when lateral deflections occur on the column. However, in the present study, column footage and beam-column joints were not casted with the column, and therefore, the resistance from membrane effects was not captured accurately, and the lateral resistance was only provided by the anchor bolts at the two column ends.

In the current field test setup, steel clamping system as shown in Figure 7 was designed to provide simple yet strong end restrain which could represent the actual column boundary in a frame structure. This design yielded acceptable results when we studied the normal strength concrete columns (not shown in the present paper) and UHPC columns in which the blast scenarios were less severe not to induce failure of boundary. However, it was noted that column constructed with UHPC demonstrated high blast resistance capability, and in order to record column failure phenomenon, very high blast

U1B after 17.5 kg TNT explosion U2B after 17.5 kg TNT explosion

Figure 6. Columns after blast loading

Figure 7. Column end boundary setup

loads i.e. more than 17.5 kg (up to 48 kg) TNT equivalence detonated at 1.5 m standoff distance were employed. Under these severe blast loading scenarios, the bolted steel clamping system failed to provide adequate end restrain. However, it should be noted that in the present study, the column made of NSC and UHPC were tested with the same testing apparatus and blast loads. Although the failure of the boundary clamping destroyed the ability of shear and membrane resistance of the boundary, which altered the failure mode of the column and made it more like a rocking column, i.e., the two ends of the column were not fixed, the comparison between NSC column and UHPC columns can provide some insight or quantitative knowledge about the blast resistance of this novel UHPC material.

The excellent blast resistance capacity of UHPC column studied in the present research is largely due to the improved concrete material performance. However, the attribution from the reinforcement is another factor not to be overlooked. In a previous study, shear dilatancy was identified as an important factor influencing response of columns under blast loads [25]. The stirrup reinforcement of columns in the present study was designed in a relatively dense layout, and they could provide restrain to the lateral dilatancy of the concrete core, and increase the shear resistance. With the aid of confinement effects from transverse steel, the failure of columns especially the concrete cores was delayed and column response became more ductile.

The test results indicate that inclusion of axial load (1000 kN) on the column yields smaller mid-span flexural deflections. Similar observations on impulsively loaded ultra-high performance steel fibre reinforced concrete column and steel tube column were also reported in [26, 27]. This is because axial load provides confinement to the concrete material and therefore applying axial load increases the flexural and shear capacity of the column if the deflection is small. When column deflection is large such that P- effect becomes prominent, axial load may cause loss of stability of the column.

Another possible reason for the strength enhancement is the membrane effect. In the present study, axial loads application provides lateral restrain to the column, and compressive membrane action may occur. As shown in Figure 8a, compressive membrane action (or so-called arching effect) occurs at the early stages of deflection. The deflection may cause a migration of the neutral axis which is accompanied by in-plane expansion of

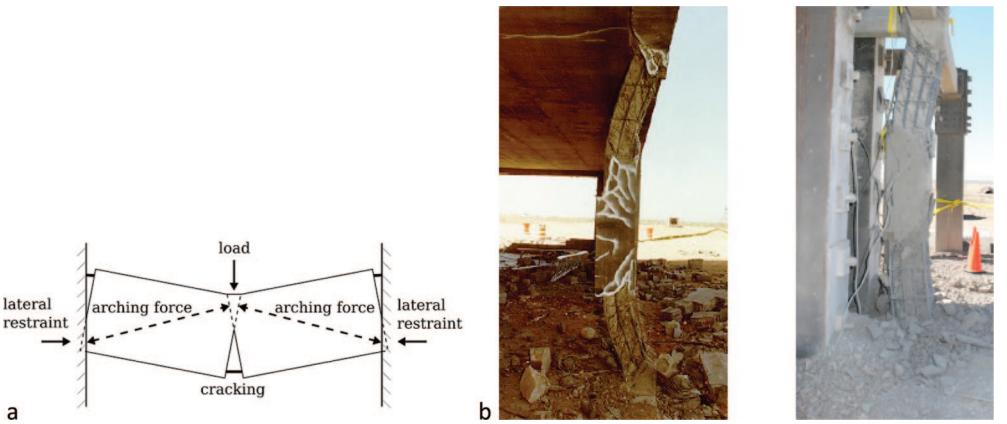

Figure 8. Typical column membrane effects (23, 24)

the column at its boundaries. If this expand is restrained, in this case by the axial load application, the development of arching action enhances the strength of the column. The compressive membrane effects can be accounted for the different column deflections under the same blast loading condition.

Compressive membrane is followed by tensile membrane action at more advanced loading stages. As the deflection of the column increases, cracking of the concrete occurs, and the column carries load by the reinforcement acting as a plastic tensile membrane. The ultimate tensile membrane capacity is reached when the reinforcement is at incipient rupture (See Figure 8b [23, 24]). In the present study, tensile membrane action is deemed of low importance because it only occurs at large deflections. By the time any significant tensile membrane is formed, the column has sustained enough residual deflection so that it will fail under subsequent axial load.

Application of axial load results in an increase in column moment capacity and nominal shear strength. Axial load also generates a compressive stress state in the column prior to the blast action, and the blast loads need to compensate the compressive stress before inducing significant flexural deflection [9]. However it should be noted that when columns experience large deflections, axial loads will amplify the lateral deflection and internal moment due to the P- effect. Although not observed in these two columns tested, it can be predicted that with further increase of the axial load and column deflection, the column will transit from a gradual stiffness and strength degradation to a rapid loss of strength due to the buckling of the longitudinal reinforcement.

4. RESIDUAL LOAD CARRYING CAPACITY TESTS

As discussed in the introduction, for a load carrying column, the critical parameter influencing the post blast performance is its residual load carrying capacity. To obtain the residual load-carrying capacities, the blast-tested UHPC columns in the current study were taken back from the field to the laboratory and tested under static loads until failure.

Figure 9 shows the sketch of apparatus for static load testing of UHPC columns. This hydraulic testing system is capable of providing a maximum axial load of 10,000 kN (1000 ton). In testing, a column was placed on top of the supports, and an axial load was gradually applied on column ends with a controlled loading rate of 1 kN/s until a constant value of 500 kN was reached. Then the axial load was kept on the column for 60 seconds

before increased again to 1000 kN and 2000 kN, respectively until failure, and at each of these loading levels the constant load maintained for 60 second as shown in Figure 10. The testing procedures were made to guarantee the hydraulic load cell in a firm contact with the column ends.

It is worth noting that in the residual loading tests, the column was placed in the horizontal position on the steel supports as shown in Figure 9 owing to the restriction of the testing equipment. This arrangement makes the specimen more like a simply-supported beam subjected to an axial force instead of a column; the two supports would also generate some

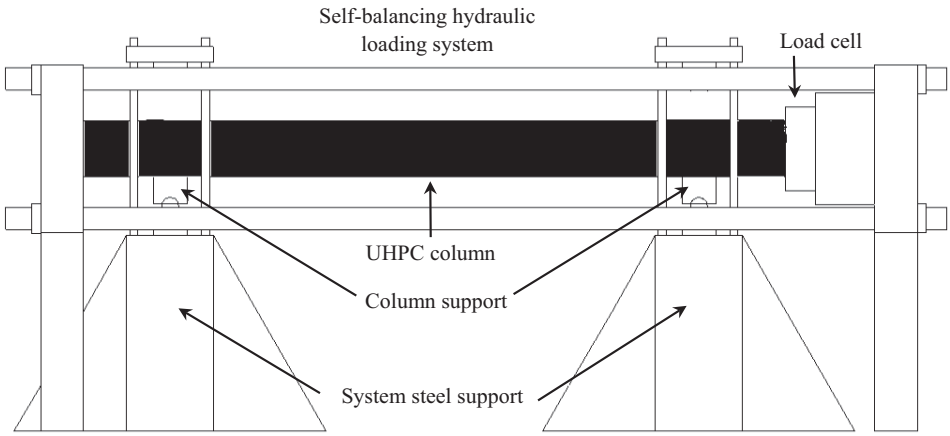

Figure 9. Column residual load carrying capacity testing system

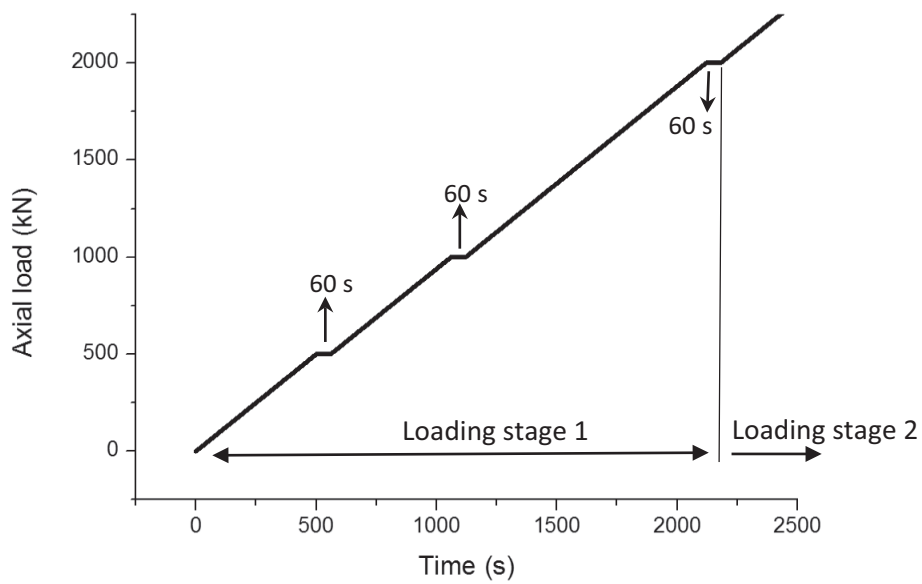

Figure 10. Loading scheme in the residual tests

constraints to the specimen to reduce the free span length of the column and a small friction force in the axial direction, which however is believed insignificant as compared to the static axial load applied. The resultant axial force within the clear loading span, i.e. between the two steel supports can be estimated by:

$$F = P - W/2 \tag{1}$$

where F is the resultant axial load, P is the axial load at column ends, W is the column self-weight and μ is the static friction coefficient between steel and concrete.

In the present study, column self-weight is around 2500 N, static coefficient between steel supports and concrete is taken as 0.2 (depending on the steel surface roughness), then the friction force at a steel support is 250 N. Compared to the failure axial load which is around 5800 kN, the influence from the supports is small and can be neglected.

Before the test on each blast damaged UHPC columns, an undamaged identical UHPC column was tested to provide benchmark load carrying capacity. For undamaged columns under axial compressive loads, there are two possible failure modes, i.e. failure due to stress exceeding the material compressive strength and buckling due to instability. For short concrete columns, they usually fail under material compressive failure while for long (or slender) columns, they usually fail due to buckling. It is critical to check intermediate-length columns like the columns in the current study to determine which factor is more critical in causing the failure.

For columns facing possible buckling, the critical load indicating the equilibrium stability limit can be simply calculated based on the Euler formula as:

$$P_{cr} = \pi^2 EI/(kL)^2 \tag{2}$$

where E is the material elasticity, I is the average moment of inertia of the cross section of the column, L is the unsupported length of the column, k is the column effective length factor, and for column with different boundary, k value varies from 0.5 to 2.

In the current test setup, both ends of the UHPC column are in firm contact with the steel load cell, and the end rotation is limited, if not fully constrained. The column effective length factor k is therefore determined to be 0.5. After substituting this value together with other parameters into Equation 2, the critical axial load for UHPC column buckling is determined as 16000 kN. Dividing this value by the cross-sectional area, a stress equals to 400 MPa is obtained and this stress is larger than the material compressive strength. The failure of UHPC column in the current study is then determined to be controlled by material compressive strength.

As shown in Figure 11, under axial loading condition, the undamaged column gradually lost load carrying capacity owing to the concrete fracture at the column support. No flexural damage at the column mid span was observed.

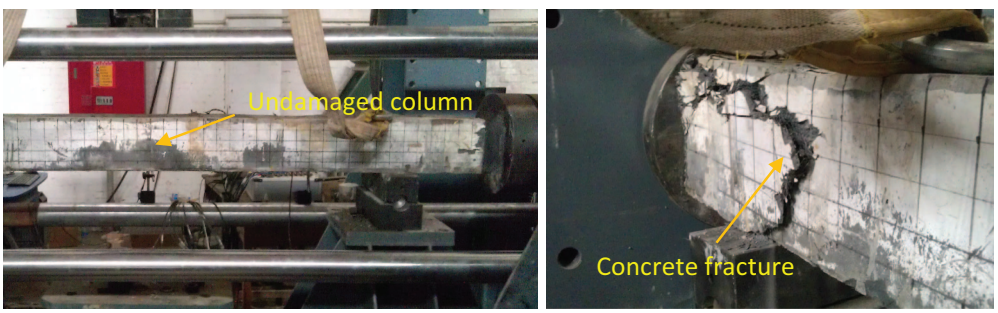

Figure 11. Test on undamaged UHPC column

In this test on the undamaged UHPC column, upon column failure, its axial load is 5900 kN. Comparing this value with the theoretical value derived from the compressive strength shown in Figure 3, which is 5920 kN, the experimental test result has very small deviations, and thus is deemed accurate. The validity and accuracy of residual load carrying test is confirmed.

Figure 12 shows U1B column after the residual load carrying capacity test, and it is clearly noted the damage mode of U1B is significantly different from the undamaged UHPC column. This is because blast load caused flexural damage at the column mid span as shown in Figure 6. The less confinement to reinforcement bars at the mid span due to concrete damage and plastic deformation of the reinforcements by blast load reduced the capacity of the section at the mid span. As a result, failure occurred at the mid span due to concrete crushing and reinforcement buckling when axial load was applied.

Figure 13 shows the failure mode of U2B due to static axial load in the residual load carrying capacity test. Similar damage mode, i.e. concrete crushing and reinforcement buckling occur at the column mid span where the initial damage from the field blast test locates.

The residual loading capacity of U1B and U2B are 5825 kN and 5660 kN, respectively, only slightly smaller than the undamaged column. Comparing with the undamaged counterpart, the load carrying capacity losses of these two columns are 1.3% and 4.1%, respectively. Both columns remain most of their load capacity. These results further demonstrate the outstanding performance of the novel UHPC material.

Figure 12. Failure of U1B column under residual load carrying capacity test

Figure 13. Failure of U2B column under residual load carrying capacity test

5. NUMERICAL STUDY

In the current study, numerical models aiming to reproduce the field blast tests and residual load carrying capacity tests are developed in LS-DYNA. Eight node hexahedron solid elements are employed for simulating the UHPC material. For the reduced integration elements, the Flanagan–Belytschko based hourglass control option available in LS-DYNA is used with the hourglass coefficient set to 0.1. Hughes-Liu beam element with cross section integration is used to model the steel reinforcement. Small element size was used in the previous study [1] to capture the highly localized damage like concrete spall under blast loads. However, in the present test observations, the primary response mode is global response and the damage is plastic deformation at the mid-span. After a convergence test, a mesh size of 10 mm is used for the finite element model.

In LS-DYNA, material models such as Pseudo Tensor (MAT_16) [28], Johnson Holmquist Concrete (MAT_111) [29] and Concrete Damage Rel3 (MAT_72_REL3) [1, 30] have been widely used for normal strength concrete modelling under dynamic loading condition [1, 31–35].

For UHPC material, Thiagarajan et al. [36] also used Concrete_Damge_Rel3 model to simulate its behaviour under blast loads, however, it was noticed that this model was developed based on normal strength concrete and therefore it is not suitable for modelling UHPC through parameter generation function. To capture the UHPC material behaviour, i.e. nonlinear softening after yielding, Teng et al. [37] and Wang et al. [38] developed a numerical model based on MAT_Elastic_Plastic_Hydrodynamic to simulate the UHPC members subjected to dynamic loads, and their simulation results showed high accuracy when comparing with the experimental observations.

In the current study, Mat_Elastic_Plastic_Hydrodynamic is employed to describe the behaviour of UHPC. This material model allows tabulated input of effective plastic stress versus effective plastic strain, and up to 16 stress versus strain values are allowed to capture the hardening and softening phase of UHPC. For UHPC material used in the present research, input plastic stress and strain values are obtained from Figure 3. Mat_Piecewise_linear_plasticity is used to model the behaviour of steel reinforcement under blast loads. Perfect bond between concrete and steel reinforcement is assumed.

Solid element erosion criterion i.e. tensile strain 0.1 is adopted in the current simulation, and this relatively large erosion criterion is applied when large element distortion happens. Ideally, element erosion should not be used as it has no physical background and massive deletion of elements breaches the mass conservation and therefore the validity of the numerical results cannot be confirmed. However when simulating large structural deformation such as their response under blast loads, erosion is unavoidable as element distortion can cause computer overflow and stops the simulation process.

It should be noted that there are some drawbacks of the current numerical simulation setup. Firstly, the dynamic material properties especially the dynamic increase factors for concrete strength were neglected. This is mainly due to the lack of material data at current stage. However, according to previous studies, it was generally noted that UHPC had less pronounced strength enhancement under dynamic loads than normal strength concrete, and neglecting dynamic strength enhancement yielded acceptable simulation results [39]. Secondly, although currently adopted material can well handle the compressive properties especially the compressive softening of UHPC, its tensile behaviour can only be captured by its tensile cutoff pressure. This simplification can inevitably bring with some discrepancies between the actual test results and the numerical simulations.

In the present study, parameters used for UHPC concrete and steel reinforcement are listed in Table 2.

Table 2. Material model and properties

Material	LS-DYNA Model	Input Parameters	Magnitude
UHPC	Elastic_Plastic_Hydrodynamic	Tabulated effective plastic stress versus strain shown in Figure 3	
	Erosion criterion	Principal tensile strain	0.1
		Mass density	7800 kg/m^3
		Elastic modulus	2.00E+11
Steel	Piecewise_linear_plasticity	Poisson's ratio	0.3
		Yield stress	1350 MPa
		Failure plastic strain	0.15

To use the Material Elastic_Plastic_Hydrodynamic, an Equation of State is required. In the present study, the Gruneisen EOS is defined. With cubic shock velocity-particle velocity, the Gruneisen equation of state defines pressure for compressed material as:

$$p = \frac{\rho_0 C^2 \mu \left[1 + \left(1 - \frac{\gamma_0}{2}\right)\mu - \frac{a}{2}\mu^2\right]}{\left[1 - (S_1 - 1)\mu - S_2 \frac{\mu^2}{\mu + 1} - S_3 \frac{\mu^3}{(\mu + 1)^2}\right]^2} + (\gamma_0 + a\mu)E \tag{3}$$

and for an expanded material as:

$$p = \rho_0 C^2 \mu + (\gamma_0 + a\mu)E \tag{4}$$

where C is the intercept of the V_s –V_p (shock velocity versus particle velocity) curve, E is the specific internal energy. S_1, S_2 and S_3 are the coefficients of the slope of the $V_s - V_p$ curve, and since the relationship of the shock wave velocity and particle velocity is often linear, only S_1 is considered in the present study; γ_0 is the Gruneisen gamma; a is the first order volume correction to γ_0; and $\mu = \rho/\rho_0 - 1$.

The parameters in the EOS used in the present study are shown in Table 3.

5.1. NUMERICAL RESULTS

In the present study, two cases i.e. U1B and U2B under 1 kg TNT and 17.5 kg TNT, are simulated using the proposed numerical model. Finite element model with mesh size 0.01 m is created in LS-DYNA and shown in Figure 14, and steel support is simulated through Mat_Rigid_Body. Contact_Automatic_Surface_to_Surface is used to describe the contact between the column and support. Default values in LS-DYNA are used to define the contact.

Table 3. Parameter for the equation of state

EOS_ Gruneisen	C_0	2100 m/s
	S_1	1.4
	γ_0	2

Figure 15 compares the mid-span deflection time history curve of U1B column under 1 kg and 17.5 kg TNT equivalent explosions. It is noted that for 1 kg TNT equivalent explosion, the numerical model captures the maximum deflection and reproduces time history curve quite well until the first peak. The slight inconsistence afterward can be explained by the fact that in the real blast test, the blast energy can be dissipated in multiple ways like column free vibration, friction between the column and boundary or surrounding medium. As shown the simulated peak response is slightly higher than the recorded one and the free vibration period is slightly longer than the column specimen, indicating the stiffness of the numerical model is probably slightly smaller than the real column. Nonetheless the numerical model gives reasonably good predictions of the column responses under blast loadings.

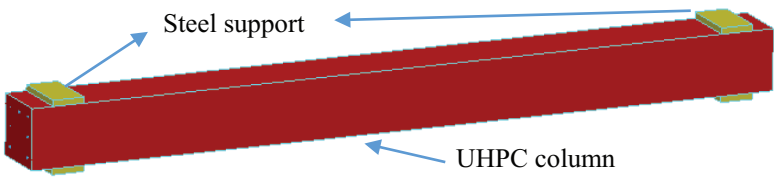

Figure 14. Finite element model

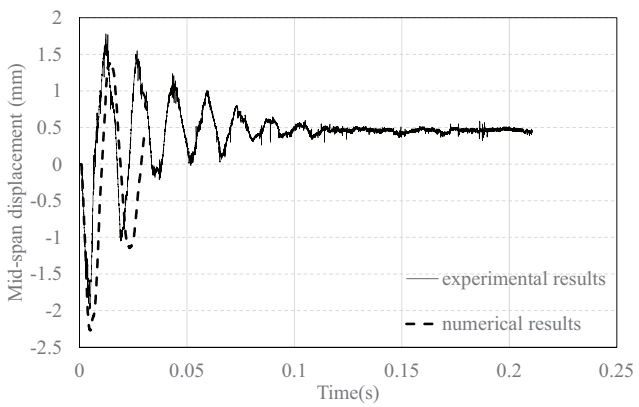

(a) U1B under 1 kg TNT equivalent explosion

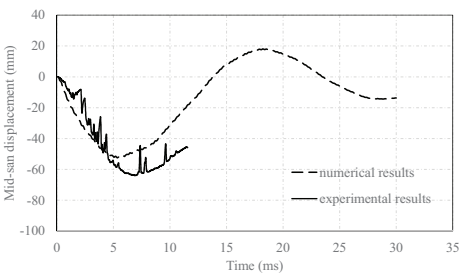

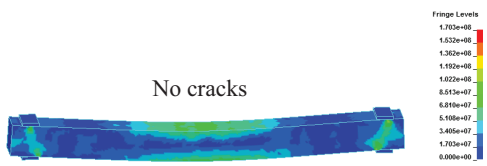

T= 5.2 ms when U1B has maximum deflection

(b) U1B under 17.5 kg TNT equivalent explosion

Figure 15. Comparison of deflection time history curve for U1B

For the 17.5 kg TNT equivalent explosion test, experimental observation gives a maximum deflection of 63.74 mm while the numerical simulation underestimates the maximum mid-span deflection of around 56 mm. The inaccurate numerical prediction can be attributed to the modelling of mid-span flexural cracks. As can be noted from the test results as shown in Figure 6, hairline cracks, although not significant, can be found on the bottom side of the column, and these cracks are quite narrow with a width less than 2 mm. In numerical simulation based on LS-DYNA, many constitutive models including Mat_10 adopted in the present study for UHPC simulation cannot model material failure. The most convenient way to model concrete crack is therefore through the erosion. Since erosion algorithm does not have physical background and should be used with caution. To avoid premature element deletion, conservative erosion criteria are usually used. For example, in the present study, a tensile strain of 0.1 is used to model UHPC material damage, i.e., crack. In reality, tensile UHPC crack might occur at a smaller strain. Furthermore, to generate small cracks with width less than 2 mm, very fine element size should be used. This requirement makes the simulation extremely time and resource consuming. If a more appropriate erosion criterion and smaller elements were used in the numerical model, larger mid-span deflection could be predicted. The current prediction underestimates the recorded deflection with an error of 12%.

For U2B column tested with 17.5 kg TNT equivalent explosion, 1000 kN axial load was applied on the UHPC column. In the numerical simulation, a static pressure of 25 MPa which equals to a 1000 kN axial load on column end cross-section is applied on one end of the column and lasts for the entire simulation. The first 10 ms is used to stabilise the column under axial load. Due to the very high axial stiffness, after 10 ms the axial velocity of the column is very small approaching zero. Therefore the effect of axial load application can be deemed negligible. Figure 16 shows the column maximum deflection at around 7.5 ms. Similar to the tested column shown in Figure 6, it is noted that at the end of simulation, no visible flexural crack is observed at the column mid-span.

Figure 17 displays the time history curve comparison for U2B column, and it can be noted that the numerical model yields a reasonably accurate maximum deflection and good time history curve prediction.

Figure 18 shows the simulation results of the undamaged UHPC column under uniaxial loading (fringe level of plastic strain is given). It should be noted that the both ends of the column model are assumed to be full fixed except axial direction, and the simple supports in the laboratory test are not included in the numerical model due to their minimal influence on the residual tests. In the simulation, a linearly increased axial load is applied on the column until its failure. The extremely high axial stiffness and slow axial loading guarantee there is no any axial vibration or velocity induced during the residual loading capacity test simulation. It is noted that the numerical simulation gives reasonable reproduction of the laboratory observation, and failure of the undamaged UHPC column initiates at the columns ends.

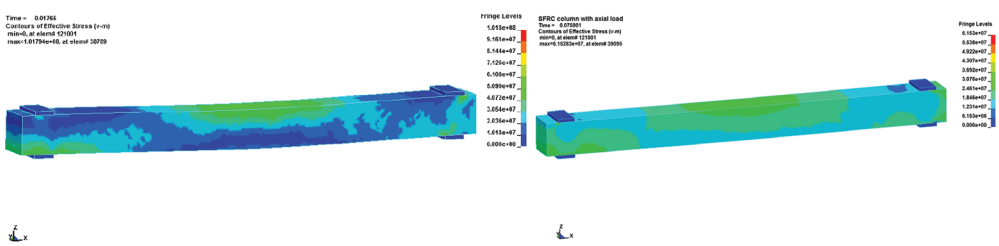

Maximum deflection Residual deflection

Figure 16. Deflection of U2B under 17.5 kg TNT

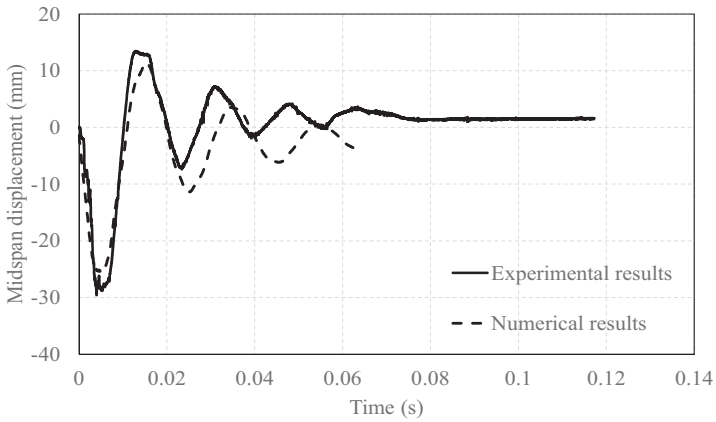

Figure 17. Comparison of deflection time history curve for U2B under 17.5 kg TNT

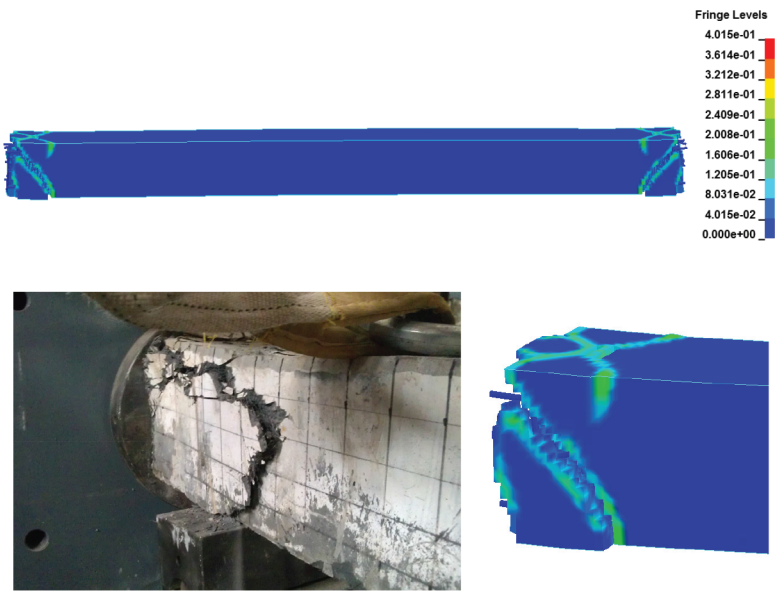

Figure 18. Simulation of undamaged UHPC column in residual load carrying test

Column residual loading capacity test of U1B column is simulated after the simulation of blast induced structural response. The simulation consists of two steps, the first is the blast response simulation as described above; and then static response simulation starts after the column residual velocity in the first step simulation becomes very small around 0.02 m/s. A linearly increased axial load is applied on the column the column failure occurs. The column residual loading capacity can then be determined. Figure 18 shows the failure mode of UHPC column U1B under residual load carrying test simulation, and it is noted U1B failure initiates at the column ends which is similar to the undamaged column as shown in Figure 11. Column lost its loading capacity when its mid span reinforcement buckled.

As shown in Figure 20, comparing with its laboratory test result, the numerical simulation of U1B column slightly overestimates the loading capacity after blast loading. This can be attributed to the fact that in the blast test simulation prior to the residual load carrying capacity simulation, the flexural cracks at column mid span are not reproduced, and these cracks influence the structural integrity and reduce loading capacity. However, it is worth noting the numerical simulation gives accurate prediction of column residual capacity which is close to 5800 kN.

Similarly, residual loading capacity test of U2B column is simulated in LS-DYNA. Figure 21 demonstrates the failure mode of UHPC column U2B under residual load carrying test simulation, and it is seen that clear concrete failure happens at the column mid span which follows the reinforcement buckling, and there is no concrete cracking at the column ends. Axial load-displacement curve shown in Figure 22 demonstrates that comparing with laboratory test results, the numerical simulation gives good predictions of the remaining load-carrying capacity of UHPC column after blast loading. In the simulation, the column fails at around 5500 kN, and comparing with the test result which is 5660, the deviation is -2.8% (positive value indicates overestimation in numerical simulation).

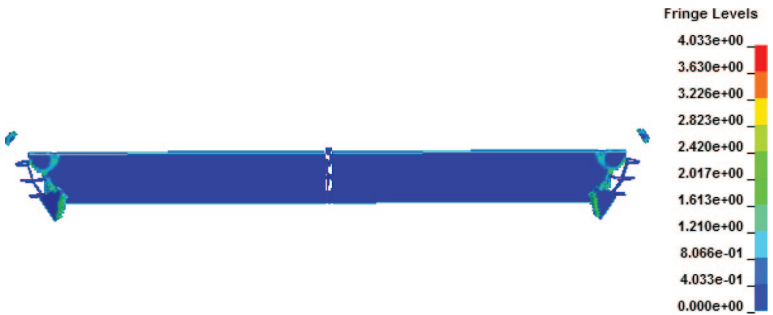

Figure 19. Failure mode of U1B column in the simulation

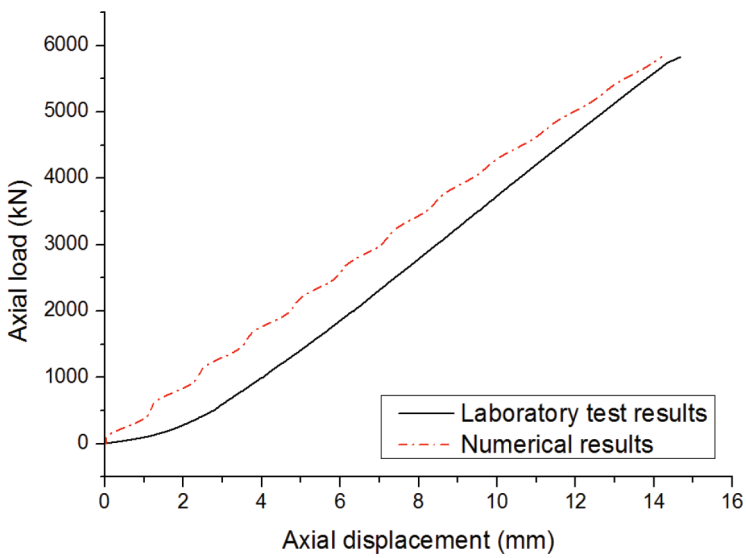

Figure 20. Axial load-displacement curve for U1B column

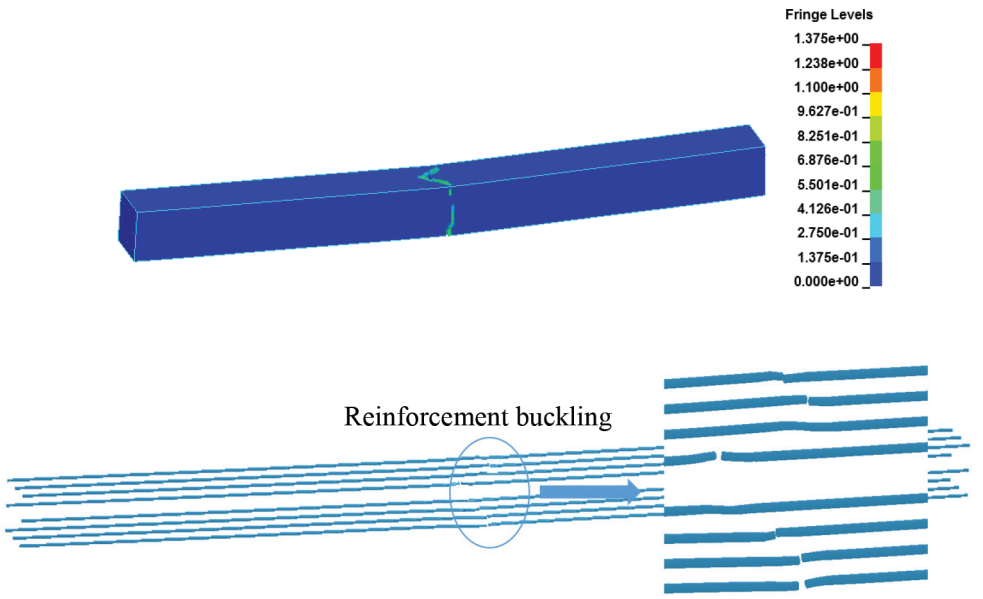

Figure 21. Failure of U2B column in residual load carrying test simulation

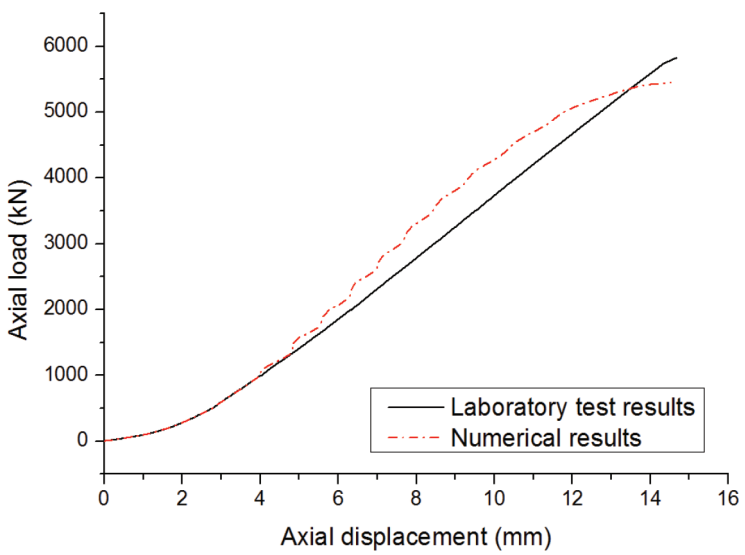

Figure 22. Axial load-displacement curve for U2B column

6. CONCLUSIONS

Ultra-high performance concrete (UHPC) is known for its ultra-high compressive and tensile strength, excellent material ductility and workability. Development of a novel UHPC material was carried out recently and nano material particles were mixed into the concrete matrix to further improve the material performance. Outstanding mechanical performance of this material under static loading condition has been demonstrated. The present study

investigates the blast resistance capacity of this newly developed UHPC material. A series of blast tests were carried out on columns built with this UHPC material. The blast damaged columns were taken back to laboratory and subjected to further static loading tests to determine the column residual loading capacity. Test results reveal that the UHPC columns retain most of their loading capacity after blast loads. Numerical models are also established to simulate the blast tests and residual load carrying capacity tests. The numerical simulation results are found to correlate well with the test results.

ACKNOWLEDGEMENTS

The research presented in this paper jointly supported by the ARC Discovery Grant DP140103025, and The National Basic Research Programme 2015CB058002 is gratefully acknowledged.

REFERENCES

[1] J. Li, H. Hao, Numerical study of concrete spall damage to blast loads, *International Journal of Impact Engineering*, 68 (2014) 41-55.

[2] T.S. Ng, A. Amin, S.J. Foster, The behaviour of steel-fibre-reinforced geopolymer concrete beams in shear, *Magazine of Concrete Research*, 65 (2013) 308-318.

[3] W. Chen, H. Hao, S. Chen, Numerical analysis of prestressed reinforced concrete beam subjected to blast loading, *Materials & Design*, 65 (2015) 662-674.

[4] P.F. Silva, B. Lu, Blast resistance capacity of reinforced concrete slabs, *Journal of Structural Engineering*, 135 (2009) 708-716.

[5] A.S. Fallah, L. Louca, Pressure–impulse diagrams for elastic-plastic-hardening and softening single-degree-of-freedom models subjected to blast loading, *International Journal of Impact Engineering*, 34 (2007) 823-842.

[6] Q. Li, H. Meng, Pressure-impulse diagram for blast loads based on dimensional analysis and single-degree-of-freedom model, *Journal of engineering mechanics*, 128 (2002) 87-92.

[7] J. Li, H. Hao, Numerical and theoretical study of concrete spall damage under blast loads, in: *Applied Mechanics and Materials*, 2014, pp. 774-779.

[8] Y. Shi, H. Hao, Z.-X. Li, Numerical derivation of pressure–impulse diagrams for prediction of RC column damage to blast loads, *International Journal of Impact Engineering*, 35 (2008) 1213-1227.

[9] X. Bao, B. Li, Residual strength of blast damaged reinforced concrete columns, *International Journal of Impact Engineering,* 37 (2010) 295-308.

[10] C. Roller, C. Mayrhofer, W. Riedel, K. Thoma, Residual load capacity of exposed and hardened concrete columns under explosion loads, Engineering Structures, 55 (2013) 66-72.

[11] O. Chaallal, M. Shahawy, M. Hassan, Performance of axially loaded short rectangular columns strengthened with carbon fiber-reinforced polymer wrapping, *Journal of Composites for Construction*, 7 (2003) 200-208.

[12] H. Hao, Z. Li, Y. Shi, Reliability Analysis of RC Columns and Frame with FRP Strengthening Subjected to Explosive Loads, *Journal of Performance of Constructed Facilities*, (2015) 04015017.

[13] M. Rebentrost, G. Wight, Investigation of UHPFRC slabs under blast loads, *Proceedings, Ultra-High Performance Fiber Reinforced Concrete 2009*, (2009).

[14] C. Wu, D.J. Oehlers, J. Wachl, C. Glynn, A. Spencer, M. Merrigan, I. Day, Blast testing of RC slabs retrofitted with NSM CFRP plates, *Advances in Structural Engineering*, 10 (2007) 397-414.

[15] B.-W. Jo, C.-H. Kim, G.-h. Tae, J.-B. Park, Characteristics of cement mortar with nano-SiO2 particles, *Construction and Building Materials*, 21 (2007) 1351-1355.

[16] Y. Qing, Z. Zenan, K. Deyu, C. Rongshen, Influence of nano-SiO2 addition on properties of hardened cement paste as compared with silica fume, *Construction and Building Materials*, 21 (2007) 539-545.

[17] X. Liu, L. Chen, A. Liu, X. Wang, Effect of Nano-$CaCO_3$ on Properties of Cement Paste, *Energy Procedia*, 16, Part B (2012) 991-996.

[18] A. Nazari, S. Riahi, The effects of zinc dioxide nanoparticles on flexural strength of self-compacting concrete, *Composites Part B: Engineering*, 42 (2011) 167-175.

[19] C. Wu, D.J. Oehlers, M. Rebentrost, J. Leach, A.S. Whittaker, Blast testing of ultra-high performance fibre and FRP-retrofitted concrete slabs, *Engineering Structures*, 31 (2009) 2060-2069.

[20] V. Bindiganavile, N. Banthia, B. Aarup, Impact Response of Ultra-High-Strength Fiber-Reinforced Cement Composite, *ACI materials journal*, 99 (2002) 543-548.

[21] J. Li, C. Wu, H. Hao, Y. Su, UNIAXIAL COMPRESSION AND FOUR-POINT BENDING ANALYSIS OF ULTRA-HIGH PERFORMANCE CONCRETE USING NUMERICAL METHODOLOGY, in: *6th International Conference on Protection of Structures against Hazard*s, 2014.

[22] J. Li, C. Wu, H. Hao, Y. Su, Investigation of Ultra-high Performance Concrete Under Static and Blast Loads, *International Journal of Protective Structures*, 6 (2015) 217-235.

[23] J. Crawford, J. Magallanes, The effects of modeling choices on the response of structural components to blast effects, International Journal of Protective Structures, 2 (2011) 231-266.

[24] J.E. Crawford, K.B. Morrill, J.M. Magallanes, Protective Design for Columns Against Close-in Blast Effects, in: *Structures Congress 2014*, ASCE, 2014, pp. 131-142.

[25] J. Crawford, Y. Wu, J. Magallanes, H.-J. Choi, The Importance of Shear-Dilatancy Behaviors In RC Columns, *International Journal of Protective Structures*, 4 (2013) 341-378.

[26] S. Astarlioglu, T. Krauthammer, Response of normal-strength and ultra-high-performance fiber-reinforced concrete columns to idealized blast loads, *Engineering Structures*, 61 (2014) 1-12.

[27] X.-L. Zhao*, Concrete-filled tubular members and connections*, 2010.

[28] L.J. Malvar, J.E. Crawford, J.W. Wesevich, D. Simons, A plasticity concrete material model for DYNA3D, *International Journal of Impact Engineering*, 19 (1997) 847-873.

[29] P. Richard, M. Cheyrezy, Composition of reactive powder concretes, *Cement and concrete research*, 25 (1995) 1501-1511.

[30] M. Deng, S.W. Shalaby, Properties of self-reinforced ultra-high-molecular-weight polyethylene composites, *Biomaterials*, 18 (1997) 645-655.

[31] J. Li, H. Hao, Influence of brittle shear damage on accuracy of the two-step method in prediction of structural response to blast loads, *International Journal of Impact Engineering,* 54 (2013) 217-231.

[32] J. Li, H. Hao, Numerical study of structural progressive collapse using substructure technique, *Engineering Structures*, 52 (2013) 101-113.

[33] J. Li, H. Hao, A Two-step Numerical Method for Efficient Analysis of Structural Response to Blast Load, *International Journal of Protective Structures*, 2 (2011) 103-126.

[34] H. Jiang, X. Wang, S. He, Numerical simulation of impact tests on reinforced concrete beams, *Materials & Design*, 39 (2012) 111-120.

[35] X. Lin, Y.X. Zhang, P.J. Hazell, Modelling the response of reinforced concrete panels under blast loading, *Materials & Design*, 56 (2014) 620-628.

[36] G. Thiagarajan, A.K. Vasudevan, S. Robert, Numerical Modeling of Concrete Slabs Reinforced with High Strength Low Alloy Vanadium Steel Bars Subjected to Blast Loads, *ACI Special Publication*, 281 (2011).

[37] T.-L. Teng, Y.-A. Chu, F.-A. Chang, B.-C. Shen, D.-S. Cheng, Development and validation of numerical model of steel fiber reinforced concrete for high-velocity impact, *Computational Materials Science*, 42 (2008) 90-99.

[38] K. Habel, M. Viviani, E. Denarié, E. Brühwiler, Development of the mechanical properties of an ultra-high performance fiber reinforced concrete (UHPFRC), *Cement and Concrete Research*, 36 (2006) 1362-1370.

[39] J. Li, C. Wu, H. Hao, An experimental and numerical study of reinforced ultra-high performance concrete slabs under blast loads, *Materials & Design*, 82 (2015) 64-76.